# REPORT DOCUMENTATION PAGE

AD-A269 091

| 1. REPORT DATE | 3. REPORT TYPE AND DATES COVERED Reprint |
|---|---|
| 20 August 1993 | Scientific   Jan 83 - Jun 93 |

**4. TITLE AND SUBTITLE**
Aircraft Observations of the Vertical Structure of
Stratiform Precipitation Relevant to Microwave Radiative
Transfer

**5. FUNDING NUMBERS**

**6. AUTHOR(S)**
A.T.C. Chang*, A. Barnes, M. Glass, R. Kakar**, and
T.T. Wilheit***

PE62101F
6870GX12

**7. PERFORMING ORGANIZATION NAME(S) AND ADDRESS(ES)**

Phillips Laboratory, GPAA
29 Randolph Road
Hanscom AFB, MA  01731-3010

DTIC
ELECTE
AUG 3 1 1993
S A D

**8. PERFORMING ORGANIZATION REPORT NUMBER**

PL-TR-93-2176

**9. SPONSORING/MONITORING AGENCY NAME(S) AND ADDRESS(ES)**

**10. SPONSORING/MONITORING AGENCY REPORT NUMBER**

**12a. DISTRIBUTION/AVAILABILITY STATEMENT**

Approved for Public Release
Distribution Unlimited

93 8 26 050

93-20022

**13. ABSTRACT (Maximum 200 words)**

    The retrieval of rainfall intensity over the oceans from passive microwave obser-
vations is based on a radiative transfer model. Direct rainfall observations of
oceanic rainfall are virtually nonexistant making validation of the retrievals
extremely difficult. Observations of the model assumptions provide an alternative
approach for improving and developing confidence in the rainfall retrievals. In the
winter of 1983, the NASA CV-990 aircraft was equipped with a payload suitable for
examining several of the model assumptions. The payload included microwave and
infrared radiometers, mirror hygrometers, temperature probes, and PMS probes. On
two occasions the aircraft ascended on a spiral track through stratiform precipita-
tion providing an opportunity to study the atmospheric parameters. The assumptions
concerning liquid hydrometeors, water vapor, lapse rate, and non-precipitating clouds
were studied. Model assumptions seem to be supported by these observation.

**14. SUBJECT TERMS**

Rainfall, Microwave, Radiative transfer, Infrared radiometer,
Particle size distributions

**15. NUMBER OF PAGES**
9

**16. PRICE CODE**

| 17. SECURITY CLASSIFICATION OF REPORT | 18. SECURITY CLASSIFICATION OF THIS PAGE | 19. SECURITY CLASSIFICATION OF ABSTRACT | 20. LIMITATION OF ABSTRACT |
|---|---|---|---|
| Unclassified | Unclassified | Unclassified | SAR |

# Aircraft Observations of the Vertical Structure of Stratiform Precipitation Relevant to Microwave Radiative Transfer

A. T. C. CHANG

*Hydrological Sciences Branch, NASA Goddard Space Flight Center, Greenbelt, Maryland*

A. BARNES AND M. GLASS

*Phillips Laboratory, Hanscom Air Force Base, Massachusetts*

R. KAKAR

*Office of Space Sciences and Applications, NASA Headquarters, Washington, D.C.*

T. T. WILHEIT

*Meteorology Department, Texas A&M University, College Station, Texas*

(Manuscript received 12 February 1992, in final form 12 August 1992)

## ABSTRACT

The retrieval of rainfall intensity over the oceans from passive microwave observations is based on a radiative transfer model. Direct rainfall observations of oceanic rainfall are virtually nonexistant making validation of the retrievals extremely difficult. Observations of the model assumptions provide an alternative approach for improving and developing confidence in the rainfall retrievals. In the winter of 1983, the NASA CV-990 aircraft was equipped with a payload suitable for examining several of the model assumptions. The payload included microwave and infrared radiometers, mirror hygrometers, temperature probes, and PMS probes. On two occasions the aircraft ascended on a spiral track through stratiform precipitation providing an opportunity to study the atmospheric parameters. The assumptions concerning liquid hydrometeors, water vapor, lapse rate, and non-precipitating clouds were studied. Model assumptions seem to be supported by these observations.

## 1. Introduction

Rain is of fundamental importance in atmospheric science. The latent heat released by rain is an important energy source for many features of the atmospheric circulation and even the dominant source in some cases. The prediction of precipitation is the major thrust of weather forecasting. Rain is the primary means by which variations in the atmosphere control our lives and the other biological processes of the earth. The importance of rain, the need for rain measurements, the present spaceborne measurement capability, and prospects for the future have all been recently discussed by Browning (1990). In the present discussion passive microwave techniques for rain measurement are the strict concern, with a full awareness that they are only a single element of any truly adequate rainfall measurement system that must include visible, infrared, and active microwave (radar) spaceborne components complemented by a wide range of ground-based measurements.

Rain is poorly measured over the earth even in well-populated regions. Over the oceans, there are essentially no measurements at all. To fill this data void over the oceans, the Electrically Scanned Microwave Radiometer (ESMR) was launched on the *Nimbus-5* satellite in 1972. The ESMR measured the upwelling thermal microwave radiation in a band centered at 19.35 GHz (1.55 cm) over a swath about 2500 km wide with a horizontal resolution of 25 km (near nadir). It was shown by Wilheit et al. (1977) that these radiance measurements could be interpreted in terms of rain rate if a reasonable height could be assigned to the freezing level. Adler and Rodgers (1978) used these ESMR data as well as the Wilheit et al. (1977) algorithm to estimate latent heat release in tropical cyclones and obtained reasonable results. Rao et al. (1976) produced an atlas of rainfall over the world's oceans using ESMR rain retrievals based on a climatology of freezing levels. They encountered difficulties in their application of the algorithm to winter rain and resorted to an ad hoc adjustment of the freezing level in order to keep

*Corresponding author address:* Dr. A. T. Chang, Goddard Space Flight Center, NASA, Code 974, Greenbelt, MD 20771.

the rain-rate retrievals reasonable. Other investigators (Tsang et al. 1977; Wu and Weinman 1984; Olson 1987; Smith and Mugnai 1988; Kummerow et al. 1989; Spencer et al. 1989; Petty 1990) also reported microwave radiative transfer calculations in the atmosphere containing cloud and rain hydrometeors in its liquid or solid form over the oceans. Unfortunately, the quantitative predictions of these theoretical models are sensitive to the details of the rain-cloud microphysics and the atmospheric structure assumed in the model. Many of these properties are still poorly known for precipitating systems over the oceans. More recently, Wilheit et al. (1991) applied this concept to the retrieval of monthly rainfall totals over the ocean areas using two frequency observations (19.35 and 22.235 GHz) from the Special Sensor Microwave/Imager (SSM/I) on the Defense Meteorological Satellite System (DMSP) satellite. In their algorithm, the Rao et al. (1976) ad hoc fix for freezing-level height was given objectively.

The lack of rainfall observations over the ocean areas both creates the need for rainfall estimates from spaceborne observations and makes the problem of validation of the estimates extremely difficult. In the absence of "rain-truth," confidence in the algorithms can be developed and the algorithms themselves improved by comparison of the details of the model on which the algorithm is based with the structure of actual rain events. Thus, the purpose of this investigation is to understand the important elements of radiative transfer processes within rain over the ocean by direct measurements within the rain column. The present investigation is only a single step towards the goal of well-founded and generally accepted rainfall-retrieval algorithms for spaceborne passive microwave observations.

The relevance of the model discussed here goes beyond the currently available data from the SSM/I and sensors from long-dead satellites. A new spaceborne experiment, the Tropical Rainfall Measuring Mission (TRMM) (Simpson et al. 1988) has been approved for a launch in the mid-1990s. Passive microwave observations are one of the cornerstones of the TRMM measurement concept. In the more distant future, the NASA Earth Observing System (EOS) *PM-1* satellite will carry a Multifrequency Imaging Microwave Radiometer (MIMR), and the Japanese Polar Orbiting Platform (JPOP) of EOS is likely to have a microwave radiometer as part of a global hydrology payload.

## 2. Background

The model [Wilheit et al. (1977), will be referred to as "the model" in this paper] used for interpreting ESMR data is indicated in Fig. 1. In the model, a Marshall–Palmer (1948) (M–P) distribution of drops was assumed from surface to freezing level (0°C isotherm). A nonprecipitating cloud layer was assumed to occupy
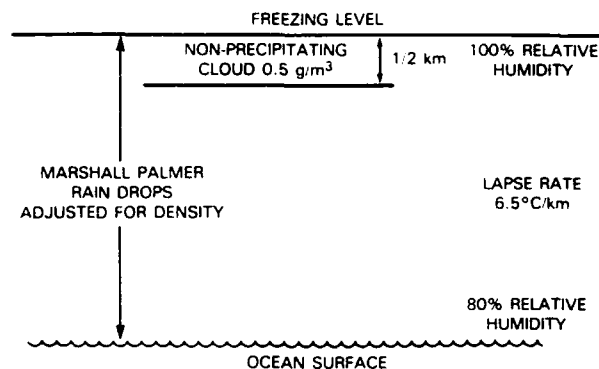


FIG. 1. Model parameters used in this study.

the 0.5 km below the freezing level and to have 25 mg cm$^{-2}$ column-integrated liquid water content. The temperature lapse rate is assumed to be 6.5°C km$^{-1}$; the surface temperature and, thereby, the freezing level, was an adjustable parameter of the model. The assumed relative humidity was 80% at the surface and increased linearly to 100% at the freezing level. The result of the model is a family of curves for a given set of viewing conditions (frequency, viewing angle, and polarization) relating rain rate to brightness temperature for various freezing levels (*R–T* relationship). The model worked quite well in accounting for the comparisons of ESMR observations with radar observations (WSR-57, Miami) and comparisons between ground-based (upward viewing) radiometers (19 and 37 GHz) and in situ rain-rate measurements (Wilheit et al. 1977). For both of these cases, the appropriate freezing level was 4 km. Later an adjustable frozen hydrometeor layer was added to the model to account for the observations at 92 and 183 GHz in intense convective rainfall (Wilheit et al. 1982). This layer is essentially invisible at the frequencies relevant to the measurement of rain over oceans (<40 GHz) under most marine circumstances.

The selection of parameters in the model, such as freezing-level height, nonprecipitating cloud-water content, relative humidity, and temperature profiles, will alter the results of the model calculations. However, a detailed sensitivity analysis of these parameters, shows that the total mass of the nonprecipitating liquid cloud drops is the most significant factor in accurately retrieving low rain rates (Chang and Milman 1982). The observations presented here allow us to address this issue. The rain-layer thickness is another critical issue. The brightness temperature is roughly a function of the product of rain rate and rain-layer thickness. Thus, a 10% overestimate in the rain-layer thickness will result in approximately a 10% underestimate in the rain rate. The relationship between the freezing level and the liquid hydrometeor thickness is one of the issues examined experimentally in this paper.

In generating their atlas, Rao and Theon (1977)

found that they obtained unreasonable results whenever the climatological freezing level was below 3 km. In those cases they found that by using 3 km as the freezing level, their monthly rainfall totals were in the range one might expect. One explanation for their difficulty could be that the climatological freezing level could be unrepresentative of raining periods, at least under mid- and high-latitude winter conditions. In the Wilheit et al. (1991) algorithm, a 19- and 22-GHz pair of brightness temperatures, which is representative of raining conditions for the 5° latitude × 5° longitude cell and month in question, is selected. The freezing level and rain rate of the Wilheit et al. (1977) model are adjusted to match the two brightness temperatures. The freezing level so derived is then used to retrieve the rainfall totals for the month for that cell. Although the result of this calculation is expressed as a freezing level, the precipitable water is the atmospheric parameter being retrieved. It is simply translated into a freezing level by the model assumptions of relative humidity and lapse rate. The observations presented in this paper enable an examination of the impact of these assumptions on the rainfall retrieval.

## 3. Experimental configuration

During January 1983, the NASA CV-990 aircraft was equipped with a collection of microwave radiometers for investigation of a wide variety of issues concerned with the remote sensing of sea ice, water vapor profiles, and rain. Those relevant to the present study consist of two radiometers that are viewed 17° to the right of zenith at 21 and 37 GHz. Just before the March 1983 portion of the experiment, a set of PMS (Knollenberg) probes were added; the observations of the 2D optical-array spectrometer cloud and precipitation probes (hereafter referred to as 2D-C and 2D-P probes) are used in the present study. The aircraft also routinely carried a Rosemount temperature probe, two- and three-stage mirror hygrometers, a nadir view-

ing PRT-5 (10 $\mu$m) infrared radiometer, and an inertial navigation system.

Two flights with this payload are relevant to the present study: 1 February and 2 March 1983. In both cases the aircraft ascended through rain areas over the oceans in a spiral flight path. For the 1 February flight, the ascent was near 40.5°N, 126.5°W over the North Pacific, and the 2 March flight was near 42.7°N, 63.5°W over the North Atlantic. The measurements are taken on an ascending rather than a descending spiral in order to prevent fogging of the various optical windows from interfering with the observations. The method is first to position the CV-990 aircraft below the cloud deck in the rain. Then the aircraft spirals up slowly (about 5 m s$^{-1}$) through the rain column with a constant roll angle of 20° to the right, resulting in a view angle of 37° for the upward-viewing microwave radiometers. Because of the constant roll angle, the diameter of the spiral increases as the altitude (and thereby the true airspeed) of the aircraft increases. On the 2 March ascent, the maximum altitude was limited to less than 9 km because of air traffic considerations.

## 4. Observations

The profiles of static air temperature and infrared temperature are shown in Fig. 2. On 1 February at the very lowest altitudes, the IR temperature was slightly above the static air temperature. The sea surface temperature (about 10°C) was approximately equal to the air temperature extrapolated to the surface. The IR temperature became equal to the air temperature at about 1 km, and they remained very close to one another up to 5 km. The IR temperature being below the static air temperature near the 4-km altitude suggests a slight calibration problem with one or the other, at least in this part of the dynamic range (near −15°C). Between 6 and 10 km in altitude, the IR temperature varied widely, indicating that the aircraft was flying in and out of broken cloud cover. The static air temper-
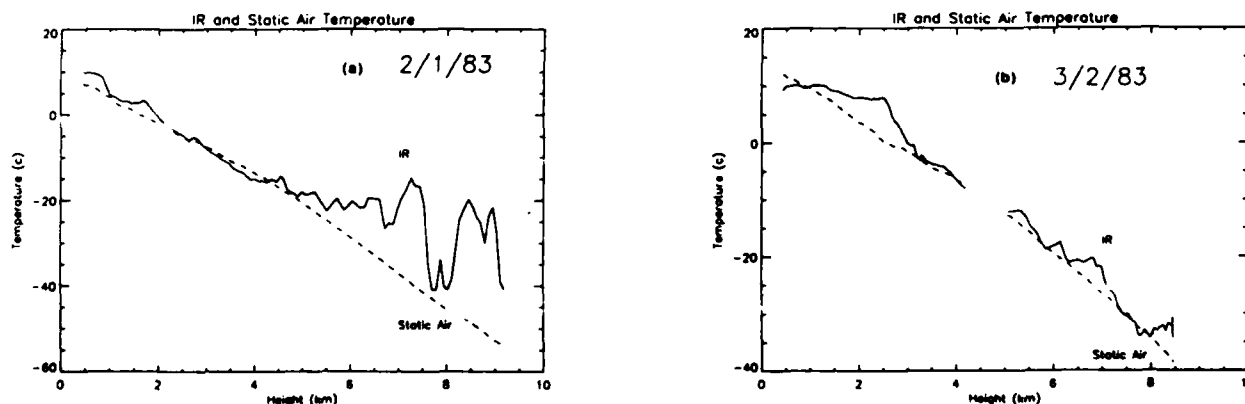


FIG. 2. Observed IR temperature and static air temperatures for the (a) 1 February and (b) 2 March cases. Infrared temperature (solid lines) and static air temperature (dashed lines).
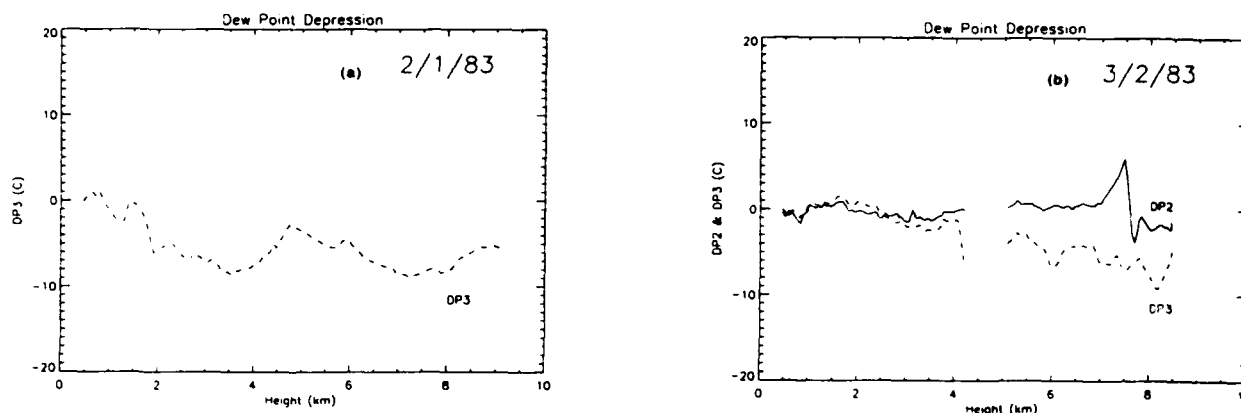
FIG. 3. Observed dewpoint depression for (a) February and (b) 2 March case. DP2 is the two-stage mirror hygrometer (solid line) and DP3 is the three-stage mirror hygrometer (dashed line).

ature decreased almost linearly with height up to 4 km with a lapse rate of 6.0°C km$^{-1}$ steepening to a rate of 8.0°C km$^{-1}$ above 4 km. The freezing level was 1.8 km, and the tropopause was at 9.8 km. On 2 March at the very lowest altitudes, the IR temperature was several degrees below the static air temperature, indicating that the sea surface temperature (again about 10°C) was less than the air temperature below 1 km. The calibration problem noted in the 1 February data is inadequate to explain this difference. The close coincidence between the IR and static air temperatures in the portions of this ascent suggests that if anything, the calibration was better on 2 March than on 1 February. The IR temperature remained nearly constant up to about 1.5 km, indicating little infrared opacity and little or no contrast between the IR and air temperatures at low levels, and it decreased only slowly from 1.5 to 2.5 km suggesting very tenuous clouds. Above 3 km, the IR and static air temperatures were generally very close, indicating almost complete cloud cover. The static air temperature decreased almost linearly with height up to 4 km, with a lapse rate of 5.7°C km$^{-1}$ and at a rate of 6.4°C km$^{-1}$ above 5 km. The freezing level was 2.5 km. Data between altitudes 4.2 and 5.0 km were lost during data recording and were not available for this study.

Figure 3 shows the dewpoint–frost-point depressions as measured by the two- and three-stage mirror hygrometers. On 1 February, the two-stage mirror hygrometer did not function properly and is not plotted. Most of the values from the three-stage hygrometer were also questionable. The dewpoint depressions up to the freezing level were fairly close to 0°C; by assuming 100% relative humidity below the freezing level the precipitable water integrates to 2.1 cm. On 2 March, the dewpoint depressions from the two- and three-stage mirror hygrometers agree quite closely from the surface to an altitude of 4 km. Above this, the three-stage hygrometer consistently indicates a negative dewpoint depression; clearly this is a malfunction of the three-

stage hygrometer. The two-stage hygrometer continues to indicate approximately saturated conditions up to a small. dry layer near 7-km altitude (−30°C). Above 7.5 km, the two-stage measurements are also doubtful, but the water vapor above this level is of little consequence for our purposes. One could assume that the relative humidity is 100% from the surface to above 8 km with very little error. Integration of the precipitable water yields a column total of 3.0 cm.

On 2 March, the cloud and rain particles were observed by PMS probes (2D-C and 2D-P). The particles were classified by shape using an automated technique (Hunter 1982), and the data were grouped into intervals of several minutes to provide sufficient samples to determine drop size distributions. Figure 4 gives the drop size distribution and gross characterization of the different particle distributions for four intervals during the ascent. The first interval (1919–1923 UTC; Fig. 4a) corresponds to the rain area below the freezing level, the second (1923–1925 UTC; Fig. 4b) represents a 600-m-thick layer above the freezing level. The third (1925–1928 UTC; Fig. 4c) is the snow layer, and the fourth (1934:30–1937:30 UTC; Fig. 4d) is characterized by small aggregates and dendrites. The diameter for nonspherical particles is assumed to be that of the circle that would have the same area as the image of the particle in the PMS data. The bulk of the particles measured in the rain region between 1 and 2 km (Fig. 4a) can be characterized by

$$N(D) = N_0 \exp\left(\frac{-D}{D_0}\right), \qquad (1)$$

where $N_0$ = 1846 m$^3$ mm$^{-1}$, and $D_0$ = 316 $\mu$m. For reference, an M-P distribution for a nominal 1 mm h$^{-1}$ precipitation rate is also plotted on Fig. 4a. Integration over the particle size distributions with the fall velocity and correction for the drag (Wilheit et al. 1977) yields computed rain rates of 1.21 mm h$^{-1}$ for the nominal 1 mm h$^{-1}$ M-P distribution and 0.94 mm h$^{-1}$ for the exponential approximation to the observed distribution
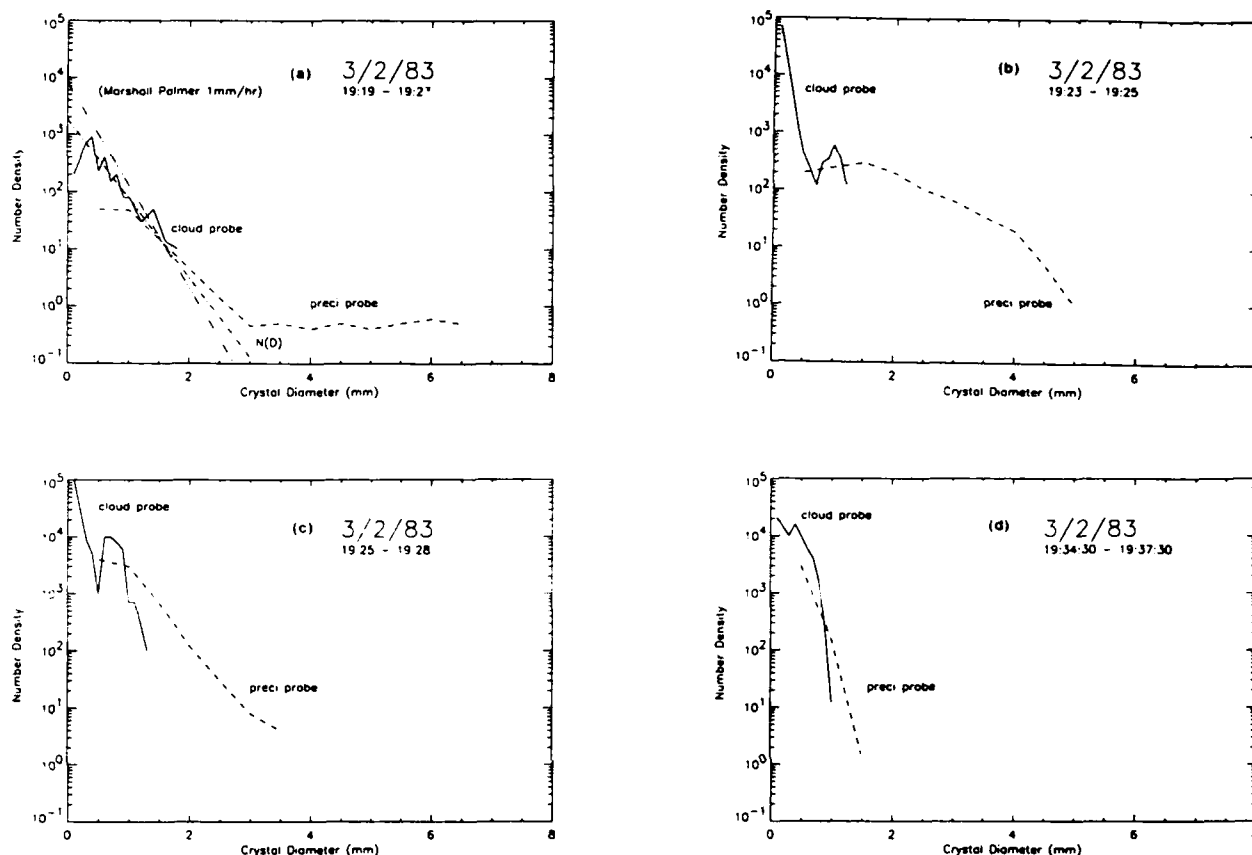
FIG. 4. Drop size distributions for the 2 March case for different time periods. (a) 1919–1923 UTC, (b) 1923–1925 UTC, (c) 1925–1928 UTC, and (d) 1934:30–1937:30 UTC. Cloud probe data (solid lines) and precipitation probe data (dashed lines). Marshall and Palmer's 1 mm h$^{-1}$ rain distribution and fitted rain distribution $N(D)$ showed in (a) for references.

[Eq. (1)]. Although the data show a tail to the distribution, at large diameters, that differs from the exponential distribution, the discrepancy amounts to less than two particles per cubic meter. More detailed descriptions of the measured particle distributions were reported by Glass et al. (1983).

Figure 5 shows the upward-viewing brightness temperatures for both frequencies (21 and 37 GHz) and for both observation days as a function of altitude. The same general features are obvious in all cases. There is a rapid and almost monotonic decrease in brightness temperature with increasing altitude from the lowest observation altitude to the freezing level followed by a more gradual decrease from the freezing level to the maximum altitude of observation. On 2 March there is also a small abrupt decrease of about 12 K at 37 GHz and 5 K at 21 GHz in brightness temperature at the 6-km altitude.

Several aspects of the Wilheit et al. (1977) model invite direct comparison with the observations. The model confines the nonprecipitating cloud to the 0.5-km layer below the freezing level. The comparisons between the static air temperature and the IR temper-

ature indicate that much, even most, of the nonprecipitating cloud is above the freezing level; the IR temperature, however, says nothing about the phase of the cloud particles. The PMS probes also measure liquid water contents of 0.58 g m$^{-3}$ for the 600-m layer above the freezing level (Fig. 4b). Also, the model assumes a lapse rate of 6.5°C km$^{-1}$; the observations suggest a range between 5.5° and 6°C km$^{-1}$. The model assumes 80% relative humidity at the surface, increasing linearly to 100% at the freezing level, whereas the observations suggest that the first several kilometers are essentially saturated. The radiative transfer computations, to be discussed in the next section, show that the exact position of the nonprecipitating cloud is a minor issue. However, the lapse rate and the relative humidity determine the relationship between the freezing level and the precipitable water, an issue with somewhat more importance.

In the Wilheit et al. (1991) algorithm, the freezing level (FL) and, thereby, the thickness of the liquid hydrometeor layer, is inferred from the retrieved precipitable water (PW). If the relationship between the PW and the FL is in error, then an incorrect liquid-hydro-
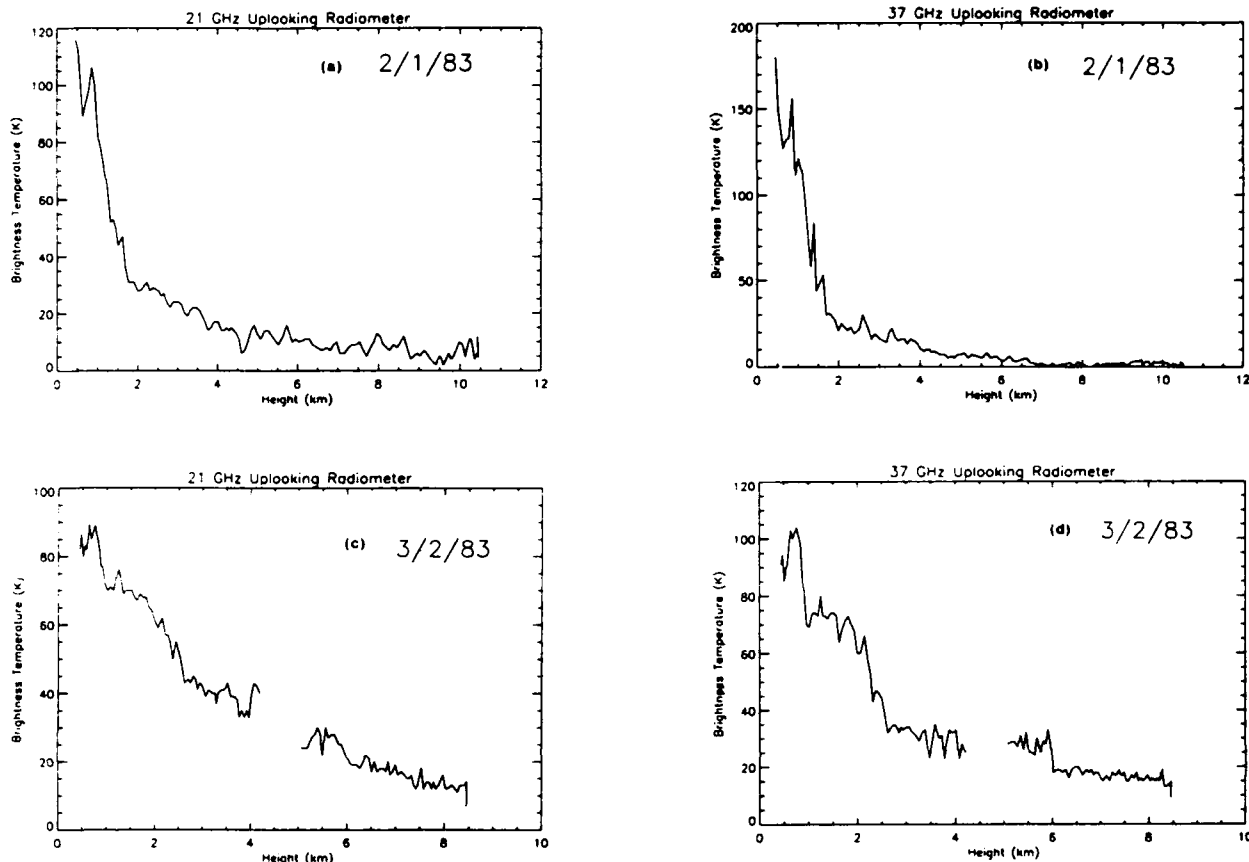
FIG. 5. Observed uplooking radiometer brightness temperatures. (a) 1 February 1983, 21 GHz; (b) 1 February 1983. 37 GHz; (c) 2 March 1983, 21 GHz; and (d) 2 March 1983. 37 GHz.

meteor layer thickness will be used in the retrieval. In Fig. 6 we have plotted the relationship between FL and PW as implied by the Wilheit et al. (1977) model (marked 80,6.5; ie., surface relative humidity, lapse rate). The specific observations of 1 February and 2 March are also shown. On 1 February essentially no error would have been made in the freezing level by application of the Wilheit et al. (1991) algorithm, but on 2 March the freezing level would have been overestimated by about 200 m. For comparison, a PW–FL relationship based on saturated conditions and a 6°C km⁻¹ lapse rate (marked 100,6) is also shown. It would have worked almost perfectly on 2 March but would have underestimated the FL by about 200 m on 1 February.

## 5. Radiative transfer computations

The brightness-temperature contributions for each of the atmospheric constituents of the model have been calculated for the uplooking radiometers and are shown in Fig. 7. The observed temperature profiles for 1 February and 2 March were used in the calculations. Since there were no in situ observations above the maximum altitude of the aircraft. there was no basis to include any constituents above that altitude. It was therefore necessary to recalibrate the brightness-temperature ob-
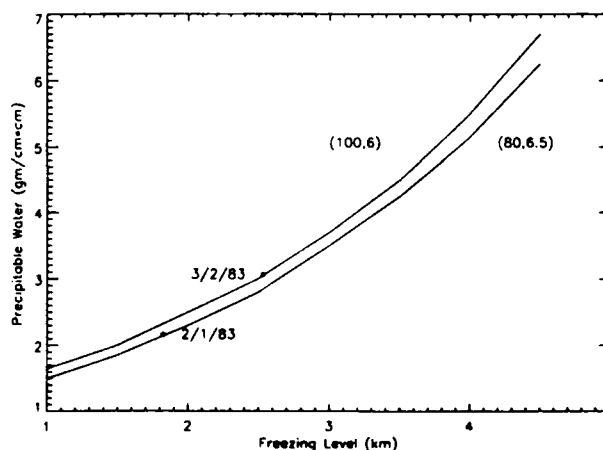


FIG. 6. Calculated atmospheric water vapor contents as a function of relative humidity and lapse rate.
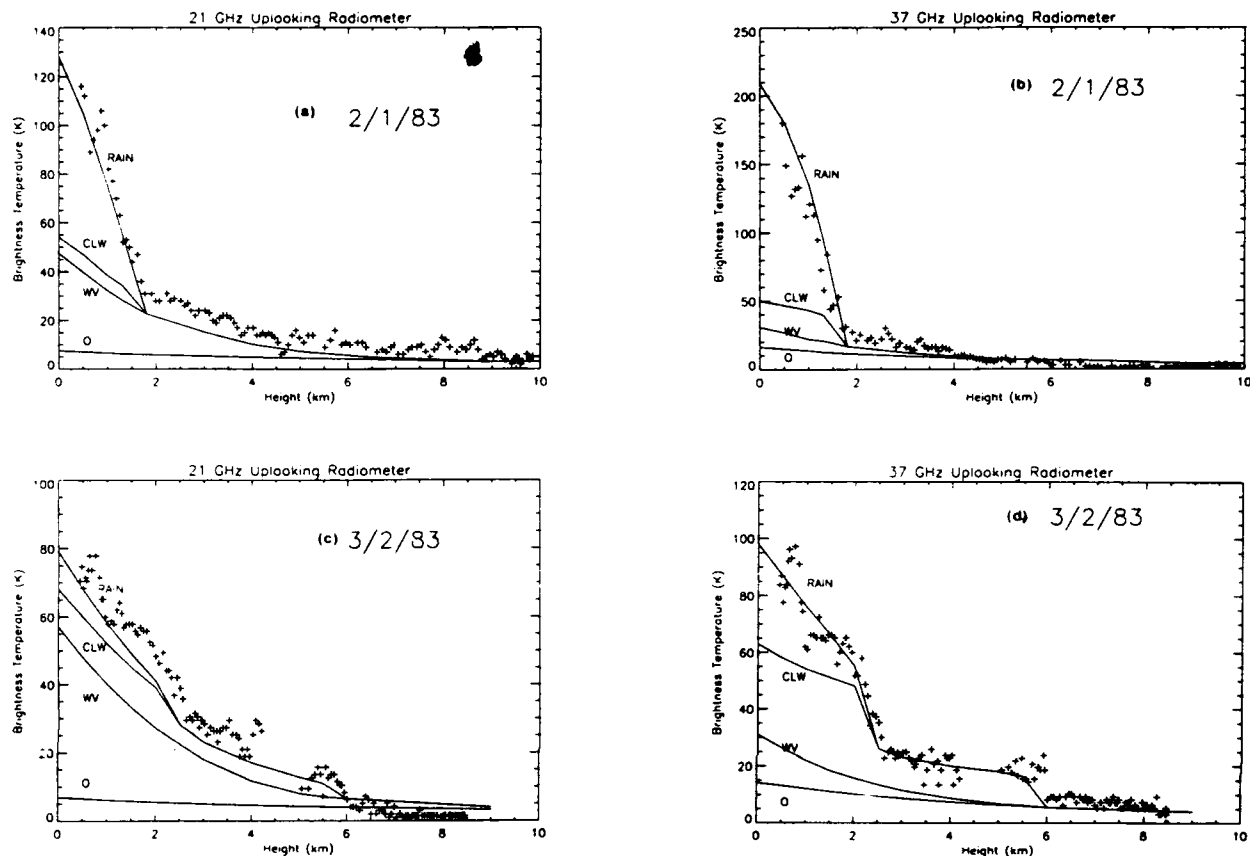
FIG. 7. Calculated uplooking brightness-temperature contributions for molecular oxygen, water vapor, cloud liquid water, and raindrops: (a) 1 February 1983, 21 GHz, (b) 1 February 1983, 37 GHz, (c) 2 March 1983, 21 GHz, and (d) 2 March 1983, 37 GHz. Observed brightness temperatures (+) are also plotted.

servations to be consistent with this limitation. These recalibrated brightness temperatures are also shown in Fig. 7. Molecular oxygen contributes only a few kelvins in the 21- and 37-GHz region. The water vapor contribution is calculated based on the observation that the relative humidity is essentially saturated to well above the freezing-level height. At 21 GHz the water vapor contribution is quite large, about 40 K for 1 February and 50 K for 2 March, due to a weak absorption line at 22.235 GHz. But its effect is rather modest at 37 GHz, 11 K for 1 February and 15 K for 2 March. The cloud liquid water and raindrops contribute the major portion of the observed radiation. Above the rain and cloud layer, the brightness temperature drops very quickly to the 3-K cosmic background.

On 1 February the FL was about 1.8 km; a cloud layer of 0.5-km thickness, containing liquid cloud of 0.5 g m$^{-3}$, was inserted between 1.3 and 1.8 km for the calculation. This cloud layer contributes 8 K at 21 GHz and 20 K at 37 GHz. On 2 March the FL was about 2.5 km, the same amount of liquid cloud was inserted between 2.0 and 2.5 km. In addition, a layer

of supercooled cloud containing liquid water of 0.2 g m$^{-3}$ was inserted between 5.5 to 6.0 km. This layer of supercooled cloud was added to mimic the abrupt change of brightness temperature observed by the uplooking radiometers.

For the 1 February case, a Marshall–Palmer distribution corresponding to 7.5 mm h$^{-1}$ was selected to match the observed brightness temperatures. For the 2 March case, the Marshall–Palmer distribution corresponding to 1.0 mm h$^{-1}$ was used. This layer of hydrometeors is clearly the dominant feature for the 37-GHz data for both days and for the 21-GHz data for the 1 February data. Due to the very light rain on 2 March, the contribution of the hydrometeors to the 21-GHz brightness temperatures is much less than the contribution of the water vapor. For the 2 March case, the computed brightness temperatures remain below the observed brightness temperatures. However, there is no supportable reason to increase the absorption in the model. This discrepancy is probably a calibration drift of the radiometer. The environmental temperature changed by some 40 K during the ascent; a calibration drift of a few kelvins would not be surprising.

The brightness-temperature contribution due to nonprecipitating cloud appears to be of about the correct magnitude for both days, but the 1 February data suggest that the cloud is distributed throughout a range of about 2 km above the freezing level, which would be compatible with the IR observations. On 2 March, on the other hand, the microwave brightness temperatures suggest that the nonprecipitating cloud is in the 0.5-km layer below the freezing level, the IR data notwithstanding.

Note that on neither day is there any abrupt change in the brightness temperature near the freezing level as one would expect for a strongly absorbing bright band. There were no radar observations to indicate the presence or absence of a bright band on either of these days, but they would not be unexpected in this type of rain. No bright band was included in the Wilheit et al. (1977) model, and these observations do not indicate the need for these two cases.

The principal use for the radiative transfer model is to provide a basis for rainfall retrievals from spaceborne observations. Therefore, the upwelling brightness-temperature change that results from several of the modeling questions suggested by these observations, the location of the nonprecipitating cloud, the additional supercooled cloud layer of 2 March, and the departure of the 2 March drop size distribution from a Marshall–Palmer distribution. These computations were performed for a range of frequencies relevant to the retrieval of oceanic precipitation using 18- and 37-GHz data. In none of the cases did the calculated brightness temperature depart from the Wilheit et al. (1977) model amount to more than 4.8 K, which would give less than 1 mm h$^{-1}$ error in the estimated precipitation rate.

## 6. Conclusions

It would be dangerous to draw broad conclusions based on such a limited set of observations. However, observations have been made of the downwelling brightness temperatures at 21 and 37 GHz, upwelling 10-$\mu$m brightness temperatures, static air temperatures, and water vapor contents in two oceanic winter rain situations. These were supplemented by PMS probe data in one of the cases. These observations have been compared with the assumptions of the Wilheit et al. (1977) model for microwave radiative transfer in precipitation. In general, the discrepancies between the observations and the model assumptions were minor. In particular, three issues have been examined.

(i) *Rain-layer thickness.* The model assumes a uniform layer of liquid hydrometeors extending from the surface to the freezing level. Although the uniformity is hard to establish from a rapidly moving platform, such as an aircraft, the liquid hydrometeors extended

from the surface to the freezing level, and nothing further is clearly established for these two cases. Certainly, there will be cases, such as strong updrafts in convective precipitation and warm rain in the tropics, where this assumption will not be met.

(ii) *Lapse rate and freezing level.* The observations suggest that an increase in the relative humidity and a decrease in the lapse rate in the model may be justified. Prudence would dictate that additional observations be considered before such a change is implemented. The impact of such a change would be in the freezing-level inference from the water vapor retrieval. The associated uncertainty appears to be of the order of 200 m, or 5% of the retrieved rainfall rate, with a 4-km freezing level—not a very large element in a total error budget.

(iii) *Cloud liquid water.* The model assumes, entirely arbitrarily, a nonprecipitating cloud containing 0.5 g m$^{-3}$ of liquid water of 0.5 km thick just below the freezing level. Although PMS probes could not delineate the phase of cloud particles, their observations for the 2 March are consistent with the assumed liquid water content to better than 50% but raise questions about the location of the liquid water. In terms of rainfall retrievals from spaceborne observations, the vertical location of the cloud liquid water is of little or no practical importance. Nevertheless, the putative liquid water at the 6-km altitude is an interesting side issue. If the brightness-temperature changes at this altitude are caused by supercooled liquid droplets or liquid-coated ice, one would expect the change at 37 GHz to be about three times the change at 21 GHz, a ratio that is consistent with the magnitudes and uncertainties of the microwave observations. On the other hand, if only ice were present, there would be no absorption, and the brightness-temperature change due to scattering would be approximately ten times as large at 37 as at 21 GHz. Such a ratio is not consistent with the observations. Others, such as Sassen et al. (1985), have suggested that supercooled water droplets are possible in cirrus clouds.

Many more observations are needed in a variety of climatological regimes before any of the observations of this paper can be generalized. Improved observations would also be a benefit. Although improvements in the calibration, noise, and reliability of the types of observations presented here would be helpful, additional observations, such as more frequencies and a precipitation radar, would be much more so. The upcoming TOGA–COARE experiment may present such an opportunity.

## REFERENCES

Adler, R. F., and E. B. Rodgers, 1977: Satellite-observed latent heat release in a tropical cyclone. *Mon. Wea. Rev.,* **105,** 956–963.

Browning, K. A., 1990: Rain, rainclouds and climate. *Quart. J. Roy. Meteor. Soc.,* **116,** 1025–1051.

Chang, A. T. C., and A. Milman, 1982: Retrieval of ocean surface and atmospheric parameters from multichannel microwave radiometric measurements. *IEEE Trans. Geosci. Remote Sens.,* **20,** 217–224.

Chiu, L. S., G. R. North, D. A. Short, and A. McConnell, 1990: Rain estimates from satellites: Effect of finite field of view. *J. Geophys. Res.,* **95,** 2177–2185.

Glass, M., C. L. Barker, and D. J. MacDonald, 1983: AFGL cloud and precipitation particle data 2 March 1983 from the NASA CV-990 for the NASA-USAF 183 GHz water vapor profiler. Air Force Geophysics Laboratory, 30 pp.

Hunter, H. E., 1982: Machine classification of cloud particle types. Air Force Geophysics Laboratory, Tech. Rep. 82-0198, 114 pp.

Kummerow, C., R. A. Mack, and I. M. Hallarinen, 1989: A self-consistency approach to improve microwave rainfall estimations from space. *J. Appl. Meteor.,* **28,** 869–884.

Marshall, T. S., and W. M. Palmer, 1948: The distribution of raindrops with size. *J. Meteor.,* **5,** 165–166.

Olson, W. S., 1987: Estimation of rainfall rates in tropical cyclones by passive microwave radiometry. Ph.D. thesis, University of Wisconsin—Madison, 292 pp.

Petty, G. W., 1990: On the response of the Special Sensor Microwave/Imager to the marine environment—Implications for atmospheric parameter retrievals. Ph.D. thesis, University of Washington, Seattle, 291 pp.

Rao, M. S. V., and J. S. Theon, 1977: New features of global climatology revealed by satellite-derived oceanic rainfall maps. *Bull. Amer. Meteor. Soc.,* **58,** 1285–1288.

——, W. V. Abbott, and J. S. Theon, 1976: Satellite-derived global oceanic rainfall atlas (1973 and 1974). NASA SP-410, Washington, D.C., 186 pp.

Sassen, K., K. N. Liou, S. Kinne, and M. Griffin, 1985: Highly supercooled cirrus cloud water: Confirmation and climatic implications. *Science,* **27,** 411–413.

Short, D. A., 1989: A statistical–physical interpretation of ESMR-5 brightness temperature over the GATE area. *Tropical Precipitation Measurements,* J. Theon and N. Fugono, Eds., Deepak, 201–206.

Simpson, J., R. F. Adler, and G. R. North, 1988: A proposed Tropical Rainfall Measuring Mission (TRMM) satellite. *Bull. Amer. Meteor. Soc.,* **69,** 279–295.

Smith, E. A., and A. Mugnai, 1988: Radiative transfer through a precipitating cloud at multiple microwave frequencies. Part III: Influence of large ice particles. *J. Meteor. Soc. Japan,* **67,** 739–755.

Spencer, R. W., H. M. Goodman, and R. E. Hood, 1989: Precipitation retrieval over land and ocean with the SSM/I: Identification and characteristics of the scattering signal. *J. Atmos. Oceanic Technol.,* **6,** 254–273.

Tsang, L., J. A. Kong, E. Njoku, D. H. Staelin, and J. W. Waters, 1977: Theory for microwave thermal emission from a layer of cloud or rain. *IEEE Trans. Antenna and Propag.,* **25,** 650–657.

Waldteufel, P., 1973: Attenuation des ondes hyperfrequences par la pluie: Une mise au point. *Ann. Telec.,* **28,** 255–272.

Wilheit, T. T., A. T. C. Chang, M. S. V. Rao, E. B. Rodgers, and J. S. Theon, 1977: A satellite technique for quantitatively mapping rainfall rates over the oceans. *J. Appl. Meteor.,* **16,** 551–560.

——, ——, L. King, E. B. Rodgers, B. Krupp, A. Milman, R. Nieman, and J. Stratigos, 1982: Microwave radiometric observations near 19.35, 92, and 183 GHz of precipitation in tropical storm Cora. *J. Appl. Meteor.,* **21,** 1137–1145.

——, ——, and L. S. Chiu, 1991: Retrieval of monthly rainfall indices from microwave radiometric measurements using probability distribution functions. *J. Atmos. Oceanic Technol.,* **8,** 118–136.

Wu, R., and J. A. Weinmam, 1984: Microwave radiances from precipitating clouds containing aspherical ice, combined phase, and liquid hydrometeors. *J. Geophys. Res.,* **89,** 7170–7178.